

A step towards digital operations - A novel grey-box approach for modelling the heat dynamics of Ultra-low temperature freezing chambers

Tao Huang^{a,*}, Peder Bacher^a, Jan Kloppenborg Møller^a, Francesco D'Ettoire^b, Wiebke Brix Markussen^b

^a*Technical University of Denmark, Department of Applied Mathematics and Computer Science, Asmussens Allé, Building 303B, Kgs. Lyngby, 8000, Denmark*

^b*Danish Technological Institute, Gregersensvej 1, Taastrup, 2630, Denmark*

Abstract

Ultra-low temperature (ULT) freezers store perishable bio-contents and have high energy consumption, which highlight a demand for reliable methods for intelligent surveillance and smart energy management. This study introduces a novel grey-box modelling approach based on stochastic differential equations to describe the heat dynamics of the ULT freezing chambers. The proposed modelling approach only requires temperature data measured by the embedded sensors and uses data from the regular operation periods for model identification. The model encompasses three states: chamber temperature, envelope temperature, and local evaporator temperature. Special attention is given to the local evaporator temperature state, which is modelled as a time-variant system, to characterize the time delay and dynamic variations in cooling intensity. Two ULT freezers with different operational patterns are modelled. The unknown model parameters are estimated using the maximum likelihood method. The results demonstrate that the models can accurately predict the chamber temperature measured by the control probe (RMSE < 0.19 °C) and are promising to be applied for forecasting future states. In addition, the model for local evaporator temperature can effectively adapt to different operational patterns and provide insight into the local cooling supply status. The proposed approach greatly promotes the practical feasibility of grey-box modelling of the heat dynamics for ULT freezers and can serve several potential digital applications. A major limitation of the modelling approach is the low identifiability, which can potentially be addressed by inferring model parameters based on relative parameter changes.

Keywords: Ultra-low temperature freezers, Grey-box models, Heat dynamics, Stochastic differential equations, Smart energy system.

*Corresponding author

Email address: taohu@dtu.dk (Tao Huang)

Nomenclature

<i>Variables and parameters</i>	T_t^w Chamber envelope temperature (°C)
C^c Heat capacity of the chamber state	$S_t(\cdot)$ Sigmoid function (from 0 to 1)
C^e A parameter determining the inertia of the evaporator	ω_t Standard Wiener process
C^w Heat capacity of the envelope state	\mathbf{X}_k The stochastic state variable of the system at time t_k
m_t Compressor state signal (0/1)	\mathbf{Y}_k The stochastic observation variable of the system at time t_k
M_t Transformed compressor state signal (-1/1)	$\mathcal{L}(\cdot)$ Likelihood function
M_t^{ac} Accumulated transformed compressor state signal	$\mathcal{L}_P(\cdot)$ Profile likelihood function
R^{ce} Thermal resistance between the chamber and local evaporator	$\ell(\cdot)$ Log-likelihood function
R^{cw} Thermal resistance between the chamber and envelope	$\ell_P(\cdot)$ Profile log-likelihood function
R^{wa} Thermal resistance between the envelope and ambient environment	<i>Abbreviations</i>
T_t^a Ambient air temperature (°C)	ACF Auto-correlation Function
T_t^c Chamber temperature measured by RTD (°C)	FDD Fault Detection and Diagnostics
T_t^e Local evaporator temperature (°C)	F#1 Freezer No. 1
$T_t^{e,in}$ Evaporator inlet temperature (°C)	F#2 Freezer No. 2
$T_t^{e,out}$ Evaporator outlet temperature (°C)	MPC Model Predictive Control
	$M_{F\#1}$ Model for Freezer No. 1
	$M_{F\#2}$ Model for Freezer No. 2
	RTD Resistance Thermal Detector
	ULT Ultra-low Temperature
	2CRS Two-stage Cascading Refrigeration System

1. Introduction

Ultra-low temperature (ULT) freezers play a vital role in pharmaceutical businesses and research organizations by preserving valuable and perishable items such as tissues, blood samples, and organs. Their significance was further underscored during the COVID-19 pandemic when ULT freezers played a critical role in storing vaccines [1]. To ensure the quality of stored contents, it is essential to have continuous monitoring and early fault detection and diagnosis (FDD) of the thermal condition in freezing chambers.

Compared to standard refrigerators, ULT freezers operate at $-40\text{ }^{\circ}\text{C}$ to $-90\text{ }^{\circ}\text{C}$. To reach low temperatures, an ULT freezer may consume up to 20 kWh/day [2]. This is estimated to be three times more than the daily power consumption of an average Danish household [3]. Consequently, ULT freezers are among the most energy-intensive pieces of equipment in hospitals, biobanks, laboratory buildings, etc. [4, 5]. Given the growing emphasis on the transition to low-carbon cities, it is also imperative to improve their energy efficiency and unlock energy flexibility [6, 7, 8]. A promising solution is to replace the simple set-point control with advanced model predictive control (MPC) [9, 10].

However, an essential prerequisite to achieving continuous monitoring, FDD, and MPC in ULT freezers is the availability of a reliable dynamic model. Previous studies have attempted to model the heat dynamics of refrigerator chambers using different approaches. They can be categorized as white-box modelling [11, 12], black-box modelling [13, 14, 15], and grey-box modelling. The deterministic white-box models are established based on detailed physical descriptions of the systems without including stochastic model parts. They are physically plausible but usually demanding to build and are not useful for statistical estimations of parameters. Black-box models are based purely on data-driven approaches. They are superior in computational load at the expense of physical interpretability. Stochastic grey-box modelling is an intermediate approach between white- and black-box modelling. Grey-box models are formulated based on physical considerations but explicitly include stochastic descriptions of unexplained variation in data. The models preserve critical physical meanings and leverage the advantage of pure data-driven approaches. The parameters can be estimated and tracked over time, which makes it possible to detect systematic changes linked directly to the operational status. Thus, grey-box models have better generalization properties than other types of models [16] and have proven to be more reliable for practical implementations [17, 18, 19, 20].

Several grey-box models for refrigerator chambers can be found in the literature. O'Neill et al. [21] modelled the heat dynamics of cold food storage rooms based on ordinary differential equations (ODEs). Leerbeck et al. [22, 23] used stochastic differential equations (SDEs) to formulate the models of the heat dynamics of supermarket refrigerator cabinets. Sossan et al. [24] and Costanzo et al. [25] modelled the heat dynamics of household refrigerator chambers and evaluated the potential to use the model for simple

MPC purposes. These models effectively capture the heat dynamics of the cold chambers. However, they rely on high-quality data from controlled experiments, which are intentionally designed to excite the systems for model identification. In addition, these models require various physical quantities as inputs apart from the temperatures, such as refrigerant flow rate, pressures at critical locations, and power consumption. These attributes demand sophisticated sensors and are difficult to measure non-invasively from the refrigeration loops. All these issues challenge the practical feasibility of these models. Even so, the literature on dynamic modelling for ULT freezers is more scarce than for standard refrigerators. Existing studies primarily focus on the pull-down performance [26, 27], theoretical thermodynamics analyses [28, 29, 30, 31], and the effects of working fluids [32, 33, 34, 35]. Due to varying settings and operational conditions, it is imperative to explore valid approaches for modelling the heat dynamics of ULT freezers.

Owing to business-critical contents, the modern ULT freezers are often outfitted with multiple temperature sensors strategically placed in the chamber and at the critical points along the refrigeration loops to facilitate maintenance and trigger warm alarms. This setup generates a vast amount of real-time temperature data from the regular operation. Considering the practical feasibility, a modelling approach, which exclusively relies on the costless data from the embedded sensors in ULT freezers, is more promising to be generalized and implemented in practice.

1.1. Challenges of using the measurements from the embedded sensors for grey-box modelling

Lumped resistance and capacitance (RC) models are a popular and effective approach to establishing grey-box models. When considering the freezing chamber as a lumped system, the temperature measured in the core region is considered representative of the global thermal condition in the chamber. In typical ULT freezers without assisting fans, the heat transfer within the chamber is dominated by natural convection, resulting in an inhomogeneous spatial temperature distribution [26, 27]. Therefore, the temperature probe used for control purposes is usually attached to the surface of the warmest part to ensure that the entire chamber is sufficiently cold, typically in the lower part of the chamber. This is mainly because the refrigerant typically enters the evaporation coil from the upper part of the freezer and exits as superheated gas from the lower part and the refrigerant used in the evaporator part of the cycle is usually a mixture temperature having a temperature glide during evaporation. Therefore, the lower refrigeration coil has a higher temperature, leading to a warmer lower chamber surface. Thus, the temperature measured by the control probe is not necessarily the mean chamber temperature but tends to be a local temperature. It has been reported in [27] that this temperature near the lower chamber surface exhibits a distinct temporal evolution pattern compared to the core region, and its dynamic response is not aligned with the states (ON/OFF) of the compressors. This may imply underlying nonlinear dynamics during heat transfer in local regions and

poses the first challenge for modelling. In addition, the natural convection causes the local surface temperature to be determined by the cooling intensity from the proximate evaporation coil. However, the cooling capacity can vary along the long coil, from the refrigerant inlet to the outlet. Consequently, the cooling input to a specific local chamber region is not constant and can vary under different practical scenarios. Thus, the model must have the capability to adapt to such local variation. This presents the second challenge when directly using the signals from the embedded sensors for grey-box modelling. Besides, the model must have acceptable complexity and a high generalisation potential.

1.2. Objectives

To this end, this study presents a grey-box modelling approach for describing the heat dynamics of the ULT freezing chamber, which has not been considered previously. The proposed grey-box modelling approach only relies on costless data from the embedded sensors. Specifically, a novel time-variant model for the local evaporator temperature is developed. The major novelty is the nonlinear part, where a time delay is modelled in continuous time. The modelling results are validated against the data from the regular operation period and residual analysis. Furthermore, we assess the model identifiability through profile likelihood and discuss a possible strategy for inferring the critical parameters to compensate for the low physical interpretability. The results from this study intend to contribute to a more practical grey-box modelling approach and thus be of use in future digital operation and dynamical monitoring of ULT freezers.

This paper is structured as follows: Section 2 provides information about the modelled ULT freezers and the data sources. Section 3 describes the modelling procedures, including detailed information about the model structure and system identification technique. The method for assessing the model identifiability is also outlined in Section 3. The results, including parameter estimates, unconditional predictions, residual analysis, and long-term model performance, along with the corresponding discussions, are presented in Section 4. This section also discusses the potential strategy for parameter interpretation, possible model applications, and associated limitations. Conclusions are followed in Section 5.

2. Descriptions of the ULT freezers and data

Two ULT freezers in regular daily use are selected for modelling in this study. Both freezers are commercial products from the same manufacturer (Thermo Scientific). Freezer No. 2 (F#2) is the predecessor of Freezer No. 1 (F#1). The selected freezers are equipped with a 2-stage cascading refrigeration system (2CRS) [36] and have an identical interior chamber dimension of $1300 \times 686 \times 1019$ mm, with four shelves. The states of the compressors (ON/OFF) are regulated based on a thermostatic control according to the temperature level measured by a Resistance Temperature Detector (RTD)

mounted on the backside of the lowest shelf, see Fig. 1. The evaporation coil uniformly winds the freezing chamber, except for the doors and bottom surfaces. The cold refrigerant flows into the evaporation coils from top to bottom of the chamber. The internal heat transfer is predominantly governed by natural convection and radiation since there are no assisting fans. Despite these similarities, the two freezers differ in the refrigerant mixtures and the types of condensers. Because of the different operational patterns, we modelled both ULT freezers to investigate if the proposed modelling strategy can be generalised to freezers with different settings. The freezers are operated by the same end-user. The defrosting of the freezer is conducted manually on a fixed schedule.

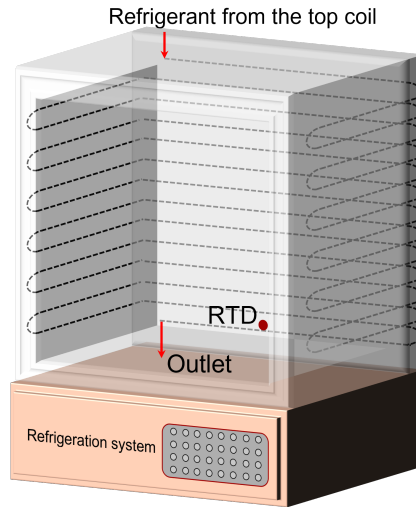


Fig. 1. Schematic of the layout of the evaporation coil and RTD. This figure is used as an illustration, so there may be a deviation from the actual conditions. The top coils are not drawn.

2.1. The data

The selected ULT freezers were situated in a room with a controlled ambient temperature. The data for modelling was recorded during regular operation periods. The thermostatic set-point of the freezers was at $-80\text{ }^{\circ}\text{C}$. A total of eight temperatures were measured. Besides RTD, the rest of the sensors were standard thermal couples and measured the inter-stage heat exchanger temperature, 1st- and 2nd-stage suction temperatures, and 2nd-stage sump temperature. Considering the model complexity, we did not model the detailed refrigeration systems and selected four temperatures for modelling, as listed in Table 1. The chamber temperature measured by the RTD is used to represent the chamber thermal condition and is hereafter referred to as RTD temperature. Although the RTD does not measure the mean chamber temperature, it is more reasonable to be used for modelling because 1) it represents the warmest, thus the worst condition, 2) the freezer is controlled based on this level, and 3) placing the temperature sensor in the core region of the chamber could reduce space efficiency and thus may not always be practical. The ambient temperature T^a was measured at the condenser air

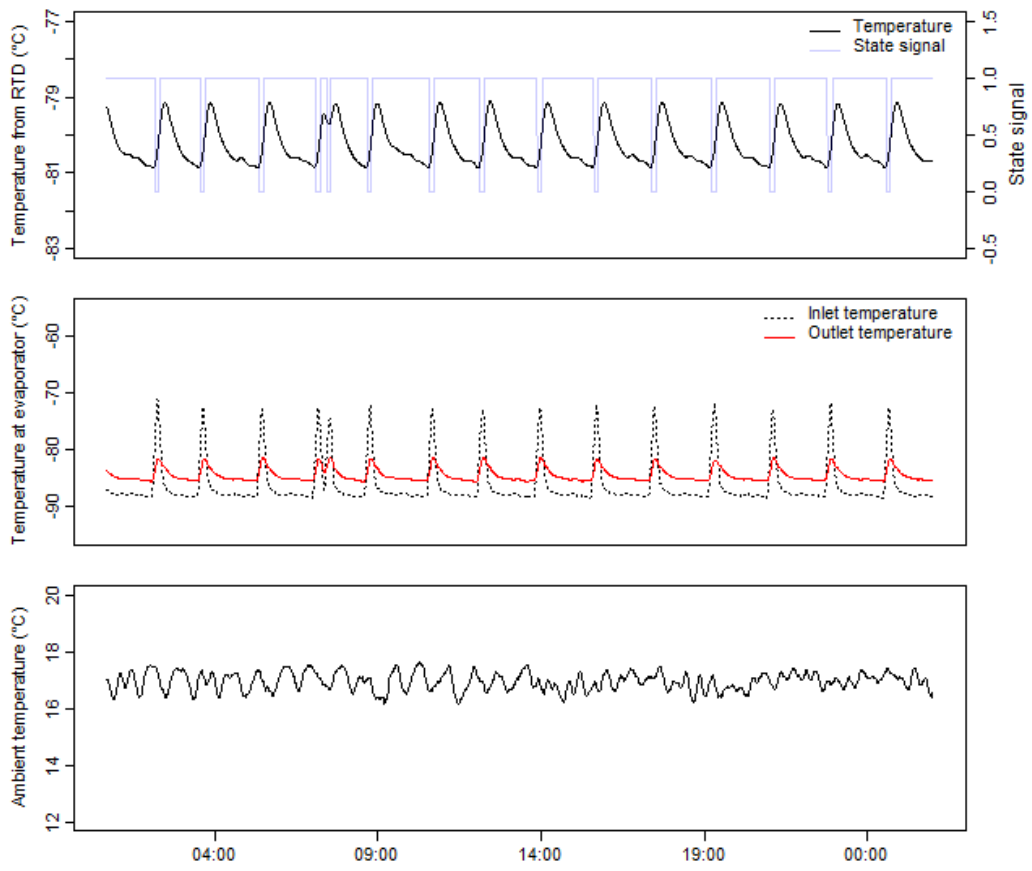
inlet. In addition to the temperatures, the compressor running state m was registered and expressed as a binary signal (OFF = 0, ON = 1). The compressor is turned on when the RTD temperature is above the set-point. This is the built-in control. Events such as door opening/closing were also logged. The temperature sensors and data logging systems are already embedded into the freezers by the manufacturer. All measurements were sampled at 1 min resolution. During the data recording period, the freezers were not emptied.

Table 1. Variables used for grey-box modelling.

Variable	Description	Unit
T^c	Chamber temperature measured by the RTD	
$T^{e,in}$	Evaporator inlet temperature	°C
$T^{e,out}$	Evaporator outlet temperature	
T^a	Ambient temperature	
m	State signal	0 / 1

Fig. 2 illustrates the time series of the temperature signals measured from the two freezers during undisturbed periods for 24 h for model identification. Undisturbed periods mean that the freezers were operating without any events occurring. The primary difference between the temperature pattern of F#1 and F#2 is the temporal evolution of the RTD temperature during the ON state. For F#1, the RTD temperature responds fast to the compressor state signal. The span of the pull-down duration is similar to that of the ON state. In contrast, the response of the RTD temperature of F#2 to the state signal is complex. When the compressors are ON, the RTD temperature rises for some time before suddenly dropping sharply. The pull-down duration of the RTD temperature is much shorter than the span of the ON state. In addition, there exists a time lag between the shifts in the compressor state signal and the response of the RTD temperature. The presented temperature profiles for F#1 and F#2 are found to be typical for the same generation of units in relation to the compressor state signals. These phenomena imply that there may be nonlinear dynamical behaviours on the cooling transport from the refrigeration loops to the local freezing chamber. Thus, directly using the compressor state signal in the model would be insufficient to express the variation in the cooling capacity. Transformations of the state signals must be performed to tackle this issue and should be discretely considered during the modelling processes. Moreover, the profiles of the evaporator inlet and outlet temperatures also differ markedly between the two freezers. The discrepancies between F#1 and F#2 could be attributed to the different settings in the refrigeration loops and actual operating conditions. Such discrepancies reveal that the operational patterns can vary significantly among ULT freezers. This highlights the imperative of developing a highly adaptive modelling approach for ULT freezers.

(a) Freezer No. 1



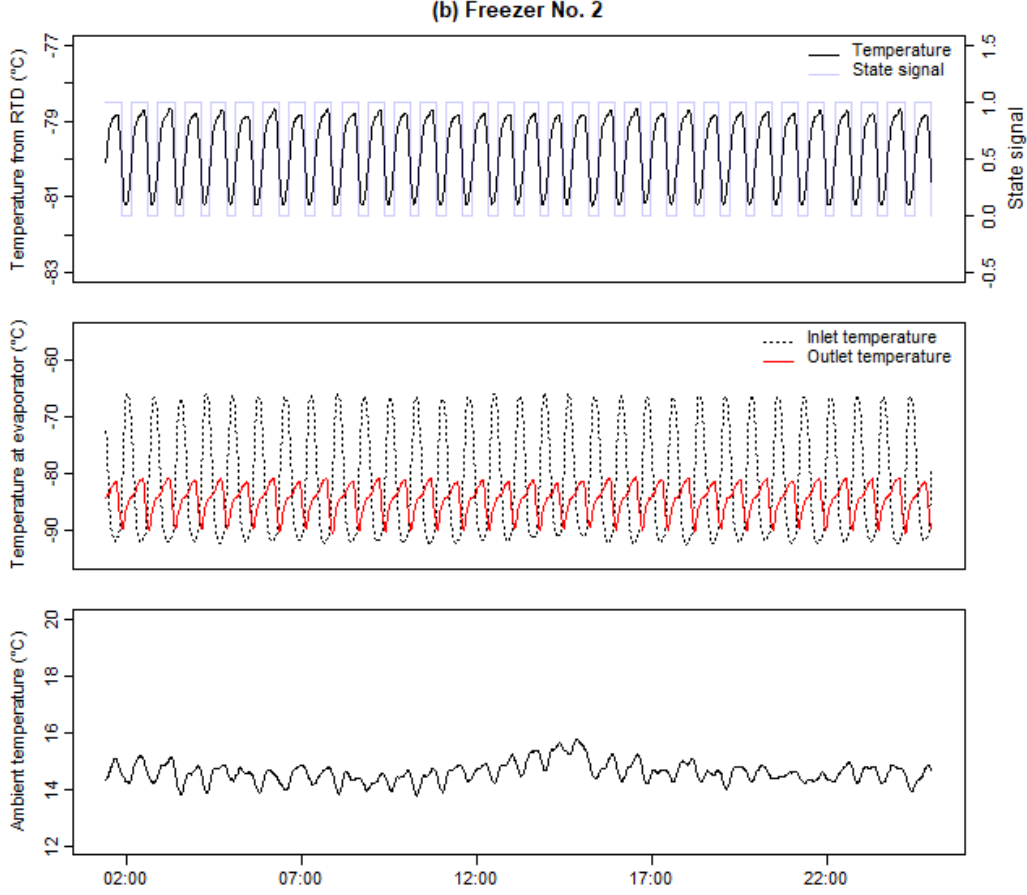


Fig. 2. Temperature profiles of the selected freezers during regular operation periods.

3. Grey-box model development

This section describes the grey-box modelling procedures. In previous models for cold storage spaces [23, 24], the exact cooling capacity or power consumption is commonly used as an input. However, flow/pressure or energy meters are not expected to be largely deployed in commercial ULT freezers because they are costly and may result in refrigerant leakage. In most prevailing cases, temperature signals are the only available measurements. Thus, the proposed approach aims to establish a model based solely on temperature measurements.

3.1. Stochastic differential equation

The proposed grey-box model is formulated using SDEs in continuous time state-space representation. The basic model structure is

$$d\mathbf{X}_t = \underbrace{f(\mathbf{X}_t, \mathbf{U}_t, t, \boldsymbol{\theta})dt}_{\text{Drift term}} + \underbrace{\boldsymbol{\sigma}_t(\boldsymbol{\theta})d\boldsymbol{\omega}_t}_{\text{Diffusion term}}, \quad (1)$$

where, $t \in \mathbb{R}$ is time, $\mathbf{X}_t \in \mathbb{R}^N$ the state vector and $\mathbf{U}_t \in \mathbb{R}^m$ is the input vector. $\boldsymbol{\theta} \in \mathbb{R}^p$ is the parameter vector. The diffusion term differentiates the

stochastic calculus from ODEs. It represents the system error and is modelled as a random walk mimicking the n -dimensional Standard Wiener processes. σ_t is the associated standard deviation. Compared to ODEs, grey-box modelling based on SDEs is more comprehensive because the diffusion terms compensate for the modelling approximations, unrecognised and unmodeled inputs by describing the stochastic nature of random errors in observed data [37].

3.2. Basic model for heat dynamics of ULT freezing chambers

The heat transfer between the ULT freezing chamber and the refrigeration system is mainly driven by the temperature gradient. The decay processes of the RTD temperature shown in Fig. 2 exhibit a pattern with a rapid initial decrease followed by a slow decrease. This suggests that the dynamics of the chamber temperature can be better captured by a second-order model, considering the presence of at least two time constants. Thus, in addition to the state of the RTD temperature, we model the chamber wall temperature as a hidden state, such that it serves as a low-pass filter between the ambient environment and the freezing chamber. The fundamental heat dynamic model of the freezing chamber is thus formulated as

$$dT_t^c = \frac{1}{C^c} \left(\frac{T_t^w - T_t^c}{R^{cw}} + \frac{T_t^e - T_t^c}{R^{ce}} \right) dt + \sigma^c d\omega_t^c, \quad (2)$$

$$dT_t^w = \frac{1}{C^w} \left(\frac{T_t^a - T_t^w}{R^{wa}} + \frac{T_t^c - T_t^w}{R^{cw}} \right) dt + \sigma^w d\omega_t^w, \quad (3)$$

where, T^c is the RTD temperature state. T^w is the chamber wall temperature state. C^c and C^w are the heat capacities of the states. R^{cw} , R^{ce} , and R^{wa} are the thermal resistances between different lumped parts. All these parameters are unknown and need to be estimated. T^e denotes the evaporator temperature and can be regarded as the cooling input in the system. Like the RTD temperature, T^e does not necessarily correspond to the mean evaporator temperature, but rather the local evaporator temperature near the RTD. Measuring this temperature can be difficult because the evaporation coil is sealed behind the chamber casing. We thus model T^e as another hidden state by leveraging the available temperature measurements at the evaporator inlet and outlet.

3.3. The time-variant dynamic model for local evaporator temperature

The local evaporator temperature T^e is modelled as an individual hidden state written as a differential equation on itself

$$dT_t^e = \frac{1}{C^e} \left(\underbrace{\left(aT_t^{e,\text{out}} + bT_t^{e,\text{in}} \right)}_{\text{hypothetical evaporator temperature}} - T_t^e \right) \cdot \underbrace{S_t(M_t^{\text{ac}})}_{\text{Sigmoid function}} dt + \sigma_e d\omega_t^e. \quad (4)$$

The drift part of the model is elaborated in the following contents. The misalignment observed between the response of the RTD temperature and the compressor state signal shown in Fig. 2 suggests a time-delayed nonlinearity in the heat transfer. Describing this feature requires addressing two issues. First, there is a time delay between the shift of the state signal and temperature drops. Such a response can be well interpreted by the thermal inertia of the evaporator, i.e., the evaporator needs to be cooled down before the heat in the chamber can be absorbed. This indicates that a buffer factor needs to be introduced to govern the inertia. We denote this factor as an unknown parameter C^e .

Second, the span of the ON state is different from that of the pull-down duration, which is particularly evident for F#2 (see Fig. 2 (b)), where the temperature drops very suddenly, and the pull-down period is much shorter than the ON state time. This indicates that the cooling capacity takes some time to reach the nominal condition, and such a process appears not linear. In previous studies [23, 24], the response of the chamber temperature is well correlated with the state signal in both starting time and duration. The discrepancy might be mainly caused by the reduced cooling capacity in the local evaporation coil as introduced in Subsection 1.1. It might also be partially due to the dual-system settings from the 2CRS. To account for the local nonlinear effect, we first conceived a hypothetical evaporator temperature, approximated as a linear combination of the evaporator inlet and outlet temperatures, i.e., $aT_t^{e,\text{out}} + bT_t^{e,\text{in}}$. The inlet temperature represents the evaporator temperature at nominal cooling capacity, while the outlet temperature is the super-heated refrigerant temperature. Depending on the scales of a and b , the resulting hypothetical evaporator temperature tends to be an intermediate temperature biased either towards the evaporator outlet or inlet, which appears reasonable. Technically, the sum of a and b should be close to 1. We intend to use this hypothetical evaporator temperature to represent an imaginary local cold source. The hypothetical temperature equals the actual local evaporator temperature if and only if the linear relationship holds. This condition is not always met because both latent and sensible heat exchanges happen in the evaporator. Therefore, a novel approach with a sigmoid function is applied to model the nonlinearity of the heat transfer on the local evaporator. The Sigmoid function writes as

$$S_t(M_t^{\text{ac}}) = \frac{1}{1 + \exp(-\alpha(M_t^{\text{ac}} - \beta))}. \quad (5)$$

A sigmoid function has a characteristic "S"-shaped curve and is parameterized by α and β , which determine the slope and the offset, respectively. Its output is bounded in the range of 0 to 1. Eq. (5) has one variable $M_t^{\text{ac}} = \sum_{m_t=0}^{m_t=1} M_t$, the accumulated transformed state signal M_t within a duty cycle. M_t is 1 or -1 according to the binary compressor state signals m_t , as

$$M_t = \begin{cases} 1, & \text{if } m_t = 1, \\ -1, & \text{if } m_t = 0. \end{cases} \quad (6)$$

The accumulated variable M_t^{ac} is reset to zero at the moment when the state signal shifts from 0 to 1, as exemplified in Fig. 3.

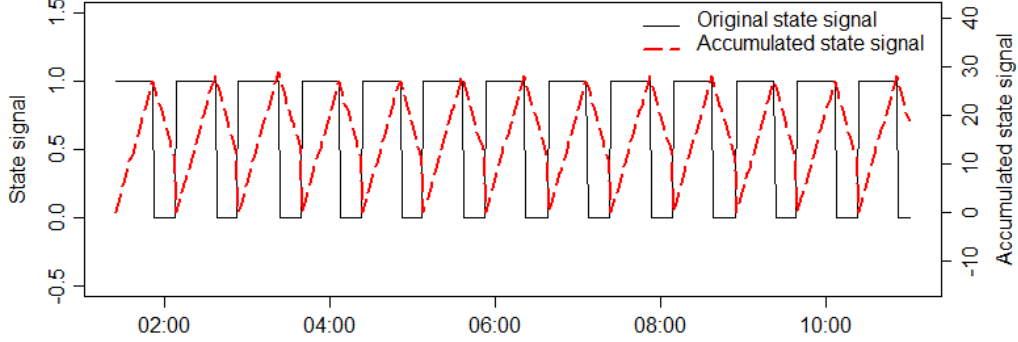


Fig. 3. An example of accumulated transformed state signal compared to the original state signal.

The parameters α and β need to be estimated along with other unknown parameters. By using appropriate values of α and β , the sigmoid function modifies the trajectory of the compressor state signal, resulting in a nonlinear smooth transition. Furthermore, we assumed that the transition between ON and OFF follows a similar variation profile. This means the same sigmoid function is applied regardless of the state of the compressors. This allows both a smooth decay and a fast increase of the modelled local evaporator temperature, as is expected in practice. Overall, the sigmoid function regulates the changing rate of the local evaporator temperature T_t^e towards the hypothetical evaporator temperature, such that the local temporal variation in the cooling intensity and nonlinear heat transfer can be described.

Eventually, the full model of the freezing chamber is formulated by Eqs. (7-9). Since none of the model parameters depends on the state variables, the model describes a 3rd-order linear time-variant system.

$$dT_t^c = \frac{1}{C^c} \left(\frac{T_t^w - T_t^c}{R^{cw}} + \frac{T_t^e - T_t^c}{R^{ce}} \right) dt + \sigma^c d\omega_t^c, \quad (7)$$

$$dT_t^w = \frac{1}{C^w} \left(\frac{T_t^a - T_t^w}{R^{wa}} + \frac{T_t^c - T_t^w}{R^{cw}} \right) dt + \sigma^w d\omega_t^w, \quad (8)$$

$$dT_t^e = \frac{1}{C^e} \left((aT_t^{\text{e,out}} + bT_t^{\text{e,in}} - T_t^e) \cdot S_t(M_t^{\text{ac}}) \right) dt + \sigma^e d\omega_t^e. \quad (9)$$

The Sigmoid function $S_t(M_t^{\text{ac}})$ represents the time-variant parameter in the system. Considering it as a whole, the model can be written as the fol-

lowing matrix form

$$\begin{bmatrix} dT_t^c \\ dT_t^w \\ dT_t^e \end{bmatrix} = \begin{bmatrix} -\frac{1}{C^c R^{cw}} - \frac{1}{C^c R^{ce}} & \frac{1}{C^c R^{cw}} & \frac{1}{C^c R^{ce}} \\ \frac{1}{C^w R^{cw}} & -\frac{1}{C^w R^{wa}} - \frac{1}{C^w R^{cw}} & 0 \\ 0 & 0 & -\frac{S_t(M_t^{ac})}{C^e} \end{bmatrix} \begin{bmatrix} T_t^c \\ T_t^w \\ T_t^e \end{bmatrix} dt + \begin{bmatrix} 0 & 0 & 0 \\ \frac{1}{C^w R^{wa}} & 0 & 0 \\ 0 & a \frac{S_t(M_t^{ac})}{C^e} & b \frac{S_t(M_t^{ac})}{C^e} \end{bmatrix} \begin{bmatrix} T_t^a \\ T_t^{e,out} \\ T_t^{e,in} \end{bmatrix} + \begin{bmatrix} \sigma^c & 0 & 0 \\ 0 & \sigma^w & 0 \\ 0 & 0 & \sigma^e \end{bmatrix} \begin{bmatrix} d\omega_t^c \\ d\omega_t^w \\ d\omega_t^e \end{bmatrix}, \quad (10)$$

where, the system state vector consists of $[T_t^c, T_t^w, T_t^e]^T$. The model input vector, the second term on the right-hand side of Eq. (10), consists of $[T_t^a, T_t^{e,out}, T_t^{e,in}]^T$. In addition, M_t^{ac} is required to calculate the Sigmoid function. Therefore, the model has a total of four inputs $\{T_t^a, T_t^{e,out}, T_t^{e,in}, m_t\}$ for performing predictions. All these four variables are continuously registered by the embedded sensors and logging systems in the ULT freezers.

We only observe T^c , so the observation equation is expressed as

$$y_t = T_t^c + e_t, \quad (11)$$

where, $e_t \sim N(0, \nu)$ is the independent and identically distributed random error from the measurements. Fig. 4 shows the simplified equivalent RC circuit of the 3-state system.

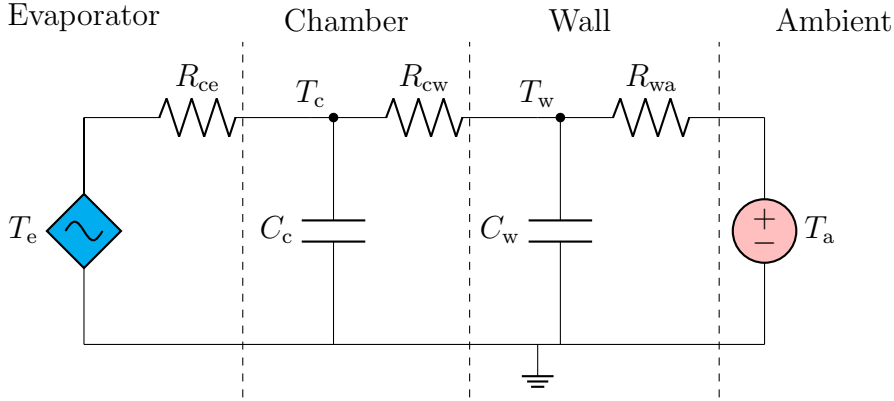


Fig. 4. Equivalent RC-network of the 3-state model. The modelled local evaporator temperature T^e acts as a controlled source.

3.4. Model identification and parameter estimation

The model parameters are estimated using maximum likelihood estimation. Given the observation sequence $\mathbf{y}_N = \{y_k\}_{k=0}^N$ and a vector $\boldsymbol{\theta}$ contains all model parameters and variances, the likelihood function is the joint probability density function (PDF) of the observations assuming that all parameters are known, expressed as

$$\mathcal{L}(\boldsymbol{\theta}; \mathbf{y}_N) = p(y_0 | \boldsymbol{\theta}) \left(\prod_{t=1}^N p(y_t | \mathbf{y}_{t-1}, \boldsymbol{\theta}) \right), \quad (12)$$

where, $p(y_0|\boldsymbol{\theta})$ is the likelihood at initial state $k = 0$. $p(y_k|\mathbf{Y}_{k-1}, \boldsymbol{\theta})$ is the conditional PDF of observing y_k given the previous observations and the model parameters. Because the increments of $\boldsymbol{\omega}$ and ν are normally distributed white noises, the conditional probability density is in the model assumed to follow the Gaussian distribution, which can be characterized by the mean and variance. Therefore, the likelihood function can be calculated using the Gaussian density function, given the one-step prediction error ϵ_k

$$\epsilon_k = y_k - \hat{y}_{k|k-1}, \quad (13)$$

where, $\hat{y}_{k|k-1}$ is the expectation of observing y_k given one-step ahead observation y_{k-1} and model parameters, i.e., $\hat{y}_{k|k-1} = \mathbb{E}[y_k|y_{k-1}, \boldsymbol{\theta}]$. The associated variance is thus $R_{k|k-1} = \text{Var}[y_k|y_{k-1}, \boldsymbol{\theta}]$. The log-likelihood function is commonly used to facilitate numerical calculations, as

$$\ell(\boldsymbol{\theta}; \mathbf{y}_N) = \log(p(y_0|\boldsymbol{\theta})) - \left(\frac{1}{2} \sum_{k=0}^N \frac{\epsilon_k^2}{R_{k|k-1}} + \log(\sqrt{2\pi \cdot R_{k|k-1}}) \right). \quad (14)$$

Eventually, the model parameters are determined by minimizing the negative log-likelihood function

$$\hat{\boldsymbol{\theta}} = \arg \min_{\boldsymbol{\theta}} -\ell(\boldsymbol{\theta}; \mathbf{y}_N). \quad (15)$$

The log-likelihood function is evaluated by calculating the one-step prediction errors ϵ_k and the associated variance R_k . The Kalman filtering approach can be used for this purpose to estimate the states. For systems with a nonlinear input, we employ the continuous-discrete extended Kalman filter (EKF) by linearizing the estimation using partial derivatives of the system and observation functions. Please refer to [38, 39, 40] for details about EKF. The data processing and scientific computing are conducted in the programming language R.

3.5. Model identifiability

The proposed grey-box model is purely informed by temperature signals. It has no dimension constraint for the thermal parameters, and the model parameters are estimated based on non-intrusive data. Consequently, the model identifiability is undermined, and some estimated parameters may lack absolute physical meanings. To assess the identifiability of the model, we calculate the correlations between estimated parameters. The calculation procedures can be found in Appendix A. In addition, we also use profile likelihood (\mathcal{L}_P). The profile likelihood is defined as the maximum likelihood estimated at fixed values of the parameters of interest [41]

$$\mathcal{L}_P(\boldsymbol{\lambda}; \mathbf{y}_N) = \sup_{\boldsymbol{\zeta}} \mathcal{L}(\boldsymbol{\theta}; \mathbf{y}_N), \quad (16)$$

where, $\boldsymbol{\theta} = (\boldsymbol{\lambda}, \boldsymbol{\zeta})$ and $\boldsymbol{\lambda}$ (p -dimensional) denotes the parameters of interest.

The profile likelihood for a practically identifiable model would show a concentrated bell-shaped distribution and an asymptotic confidence interval for all parameters. For a model lacking identifiability, the profile likelihood distribution is anticipated to be flat, meaning different sets of parameters can result in a similar likelihood. Consequently, the parameters may not be able to be associated with any physical proprieties in an absolute way. The profile likelihood-based 95% confidence interval is defined as

$$\left\{ \boldsymbol{\lambda}; \frac{\mathcal{L}_P(\boldsymbol{\lambda}; \mathbf{y}_N)}{\mathcal{L}(\boldsymbol{\theta}; \mathbf{y}_N)} > \exp\left(-\frac{1}{2}\chi_{0.95}^2(p)\right) \right\} \Rightarrow \left\{ \boldsymbol{\lambda}; \ell_P(\boldsymbol{\lambda}; \mathbf{y}_N) > \ell(\boldsymbol{\theta}; \mathbf{y}_N) - \left(\frac{1}{2}\chi_{0.95}^2(p)\right) \right\}, \quad (17)$$

where, ℓ_P is the profile log-likelihood.

4. Results and discussions

4.1. Parameter estimates

Table 2 presents the estimated parameters for the models for F#1 ($M_{F\#1}$) and for F#2 ($M_{F\#2}$). All parameters are statistically significant, except for C^e in $M_{F\#2}$ ($p \approx 0.1$). C^e governs the hysteresis between the modelled evaporator and RTD temperatures. Thus, it is believed to be necessary for the model. The weak significance might be due to the limited information contained in the data regarding the dynamics of the local evaporator temperature and the poor quadratic approximation of the log-likelihood, leading to errors in the Wald Confidence Interval. It could be found that the scales of some of the parameters differ markedly between the two freezers. For instance, R^{wa} for $M_{F\#1}$ is much higher than that for $M_{F\#2}$, while R^{cw} for $M_{F\#1}$ is much smaller than that for $M_{F\#2}$. Similar issues can be found in C^c and C^w . In a physical consideration, a plausible explanation for this can be that the heat resistance R^{wa} for $M_{F\#1}$ is the total resistance of the freezing chamber and the interior contents. In contrast, the heat resistance of the interior contents is included in R^{cw} for $M_{F\#2}$. The same explanation also applies to the discrepancy in C values. In a statistical consideration, this implies that some parameters are not independent, and the models lack identifiability. Thus, the parameters may not be physically interpretable and should not be directly compared across models. This issue will be further discussed in Subsection 4.5.

Table 2. Estimated parameters for Model No. 1 and No. 2.

Parameter	$M_{F\#1}$	95% CI	$M_{F\#2}$	95% CI
a	4.78e-5	[4.0e-5, 5.6e-5]	0.83	[0.83, 0.84]
b	0.98	[0.98, 0.99]	0.12	[0.12, 0.13]
C^c	1.54	[0.46, 1.62]	15.58	[8.37, 22.78]
C^w	11.53	[8.09, 14.97]	0.35	[0.26, 0.44]
C^e	0.11	[9.8e-2, 0.11]	2.9e-3	[-5.9e-4, 6.4e-3]
R^{wa}	13.38	[12.05, 14.70]	0.30	[0.21, 0.39]
R^{ce}	0.55	[0.55, 0.56]	1.5e-2	[0.01, 0.02]
R^{cw}	0.20	[0.19, 0.21]	9.30	[5.37, 13.23]
α	0.37	[0.30, 0.43]	0.21	[0.17, 0.26]
β	4.96	[4.45, 5.46]	25.77	[16.88, 34.67]

It is worth discussing the parameters a and b because they somewhat indicate the mixture refrigerant properties, thereby the level of the cooling intensity. In both models, $a + b \approx 1$, suggesting that a and b are self-bounded and negatively correlated. a is so small that to be insignificant for $M_{F\#1}$, suggesting that the local evaporator temperature is very close to the inlet temperature. This indicates that the evaporation effect is still intensive near the RTD. In contrast, $a = 0.83$ in $M_{F\#2}$, indicating that the local evaporator temperature around the RTD is closer to the outlet temperature of the superheated gaseous refrigerant. Therefore, the cooling intensity around the RTD is significantly reduced. Hence, the lower chamber receives reduced cooling capacity. This phenomenon partially explains the mismatch between the compressor state signal and RTD temperature evolution in $F\#2$.

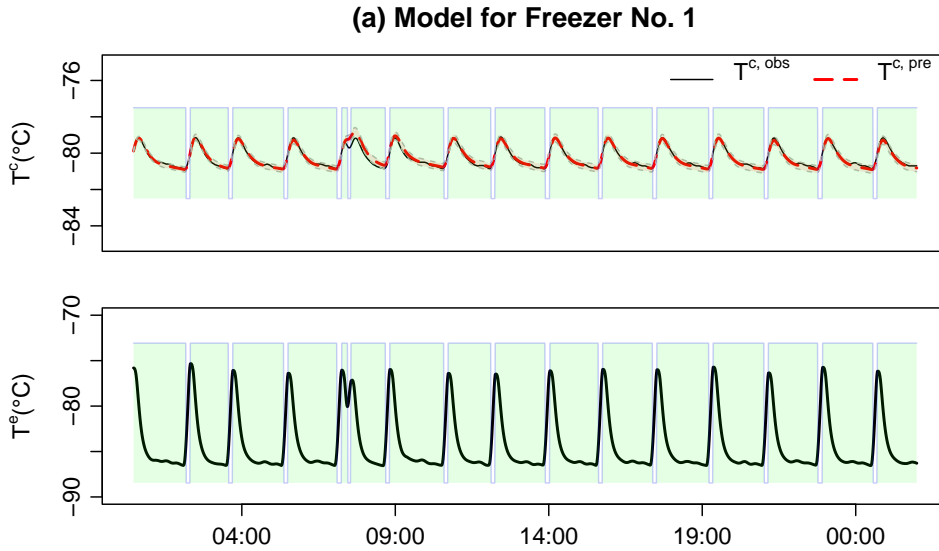
In addition, the large discrepancy between a and b indicates that the local evaporator temperature does not reflect the average evaporation temperature, supporting that the RTD temperature may not represent the mean chamber temperature. This can be a common feature for ULT freezers without assisting fans, in which the RTD temperature can often be higher than the mean chamber temperature due to reduced cooling capacity. This, on the one hand, leads to modelling challenges as mentioned in Subsection 1.1, and precludes the possibility of using global information directly as model inputs. On the other hand, it implicates that modelling global heat dynamics may risk an underestimation of the temperatures in local regions of the freezing chamber. Thus, it is crucial to avoid using such models for monitoring the thermal condition in ULT freezers.

Furthermore, the level of cooling inputs near the RTD is expected to vary under different practical scenarios, which can be attributed to variations in the mass quantities and spatial distribution of the loaded contents. Describing such variations using partial differential equations with detailed boundary conditions would be possible but significantly increase the model complexity. The proposed approach overcomes these issues by adjusting a and b values to adapt to different practical scenarios. This approach ameliorates the representation of the local evaporator state without over-complicating the

model.

4.2. Unconditional predictions

Unconditional prediction is conducted to assess the model predictive performance. Unconditional predictions of the state variables $\mathbf{T}_t|\mathbf{T}_0$ are generated by inputting the model with the initial values of three states $\{T_0^c, T_0^w, T_0^e\}$ and actual measured input variables $\{T_t^a, T_t^{e,in}, T_t^{e,out}, m_t\}$ using EKF without updating. Fig. 5 shows the predicted RTD temperature from the two freezers. The predictions agree well with the measurements, and the narrow prediction intervals indicate that the predictions are relatively accurate. The root mean squared error for $M_{F\#1}$ and $M_{F\#2}$ are $0.11\text{ }^\circ\text{C}$ and $0.19\text{ }^\circ\text{C}$, respectively. The results demonstrate that the model captures the most critical dynamics of the freezing chambers. However, the small reduction at 07:00 in F#1 is not accurately reproduced by the predictions. This reveals that some underlying dynamics are still not accounted for in the model. Identifying these dynamics would require more data containing such infrequent phenomena, which may not be worth considering explicitly.



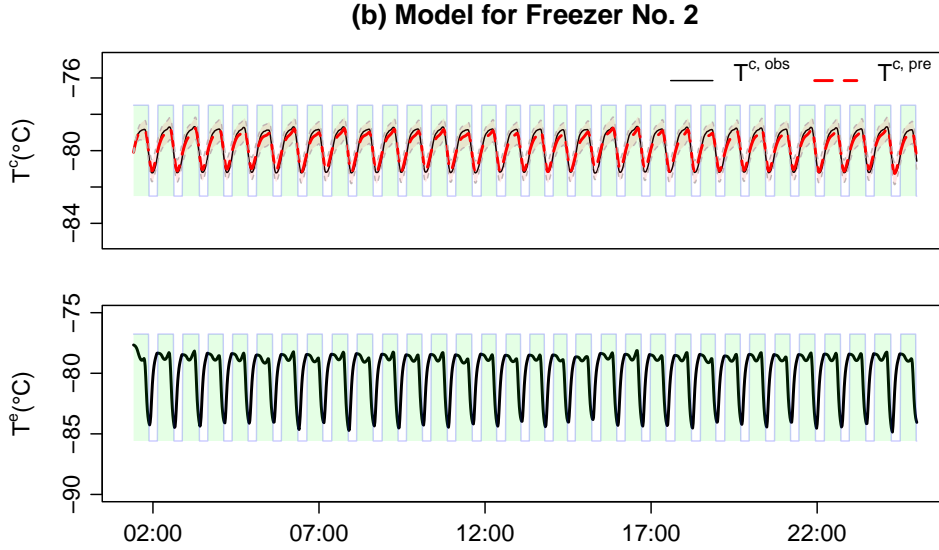


Fig. 5. Comparisons between the observations (T^c, obs) and the unconditional predictions (T^c, pre) for (a) $M_{F\#1}$ and (b) $M_{F\#2}$. The red shading areas stand for the 95% confidence intervals of the prediction results. The compressors are running during the square-shaded periods.

The predicted local evaporator temperatures are also presented in Fig. 5 and exhibit distinct patterns for the two freezers. For F#1, the overall local evaporator temperature evolution closely resembles a classical exponential decay process. It drops as soon as the compressors are ON, indicating that the evaporator is cooled down efficiently. This consequently leads to a fast decay in the RTD temperature. In contrast, the profile of the local evaporator temperature for F#2 is complex. When the compressors are turned on, the local evaporator temperature undergoes a short-term and slow reduction followed by a slight increase. During this period, the local evaporator temperature remains relatively stable. Then, a sudden and sharp reduction occurs. This pattern may appear to contradict the practical understanding of refrigeration processes but well elucidates the mismatch between the RTD temperature drop and the state signal for F#2. One possible explanation for this phenomenon is the presence of unmodelled dynamics between the evaporator and the RTD. Hence the model attempts to capture the holistic dynamics of the local evaporator and the unrecognised medium. The unmodeled dynamic process can be, for instance, due to an inadequate synergy between the compressors at the two stages. Another potential reason could be attributed to the thermal couples used to measure the evaporator temperatures. It is possible that either the installation positions are inappropriate or the time constant of the thermal couples is too high to respond adequately to temperature changes. Despite this, the patterns of the RTD temperature indeed demonstrate an inefficient and delayed cooling period during the initial ON states. The modelled local evaporator temperature effectively introduces this

delay and limited cooling capacity. In this light, the simulated local evaporator temperature still provides valuable insights into the patterns of the RTD temperature and sheds light on the possible underlying nonlinear heat transfer processes between the refrigeration system and the freezing chamber.

In previous studies on modelling refrigerators [11, 21, 24], the responses of the chamber temperature to the compressor state signal are generally consistent with what is observed for F#1. Therefore, the direct use of the state signal in conjunction with global cooling capacity for model identification can be informative. However, the operational pattern for F#2 is rarely reported and can be challenging to model using a time-invariant system without considering the nonlinear heat transfer. The results demonstrate that the proposed grey-box modelling approach can effectively capture the most crucial dynamic behaviours of the ULT freezing chambers without requiring detailed knowledge of all the underlying phenomena. Moreover, the prediction results across different operational patterns indicate that the model performance is not ULT freezer dependent, confirming the desired transferability of the proposed modelling approach for various ULT freezers.

4.3. Residual analysis

For an SDE-based model, the residuals from the estimation should be uncorrelated to prove that the model describes all auto-correlation of the systems [42]. As shown in Fig. 6 (a), the auto-correlation function (ACF) of the one-step prediction residuals for $M_{F\#1}$ and $M_{F\#2}$ are close to being white noise, despite minor spikes in some lags. The cumulated periodograms (CP) presented in Fig. 6 (b) mostly lie inside of the confidence interval but exhibit slight periodicity, implying that some dependency from the inputs still exists. Moreover, a strong auto-correlation at lag 10 can be observed in the ACF for both models, suggesting that the way of introducing certain inputs does not effectively capture this periodic phenomenon. In general, the residual analysis suggests that the models can be relied upon for forecasts, which is the backbone for reliable MPC applications.

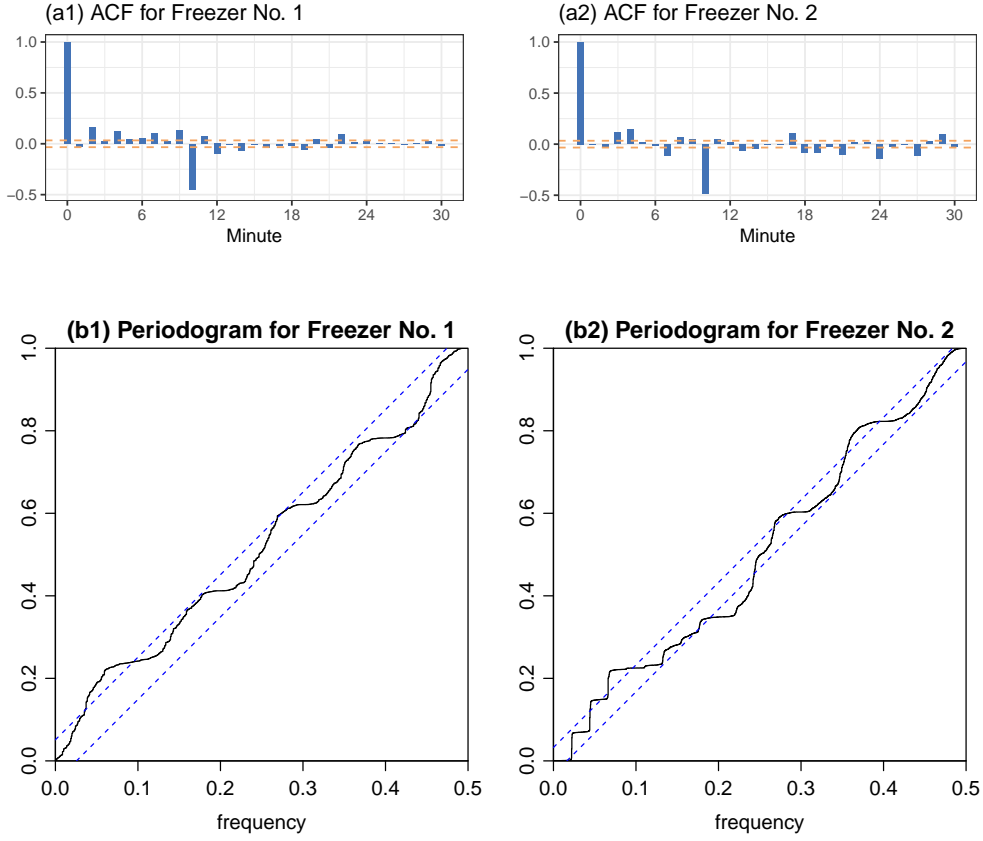
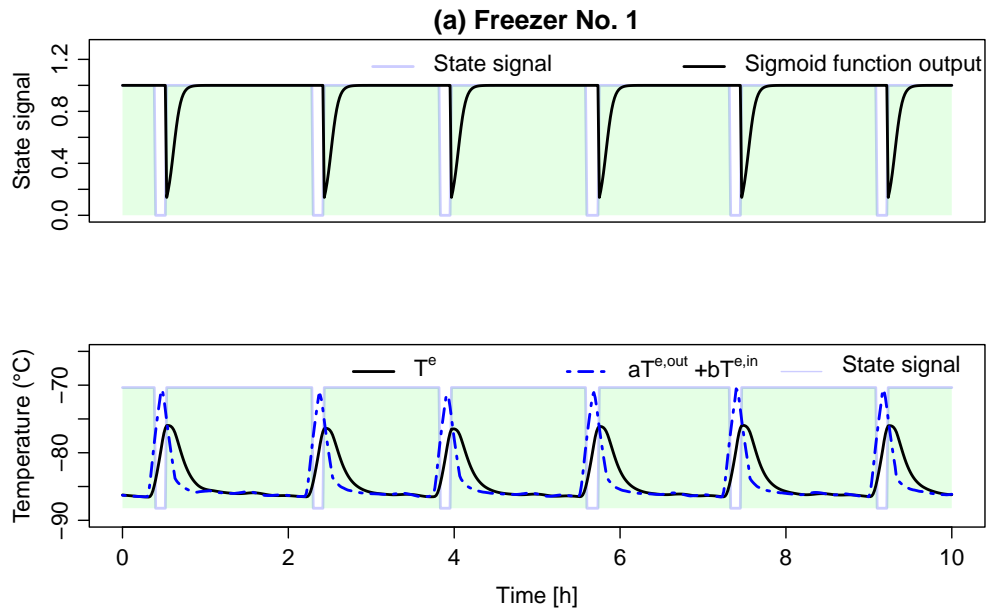


Fig. 6. (a) The estimated auto-correlation function of the one-step prediction errors and (b) cumulated periodogram for $M_{F\#1}$ and $M_{F\#1}$. The regions between the dashed lines are the 95% confidence intervals under the hypothesis that the residuals are white noise.

4.4. Effects of the sigmoid function

One of the major novelties of this study is to model the underlying nonlinear phenomena in the freezing chamber using a sigmoid function. Fig. 7 shows the trajectory of the sigmoid function along with the comparisons between the hypothetical evaporator temperature $aT_t^{e,\text{out}} + bT_t^{e,\text{in}}$ and the estimated local evaporator temperature T^e . For F#1, see Fig. 7 (a), the sigmoid function transforms the initial part of the ON state to be a smooth increase. During this transition, the increasing rate of the modelled local evaporator temperature is restricted. Due to the relatively short OFF duration, the sigmoid function keeps saturated when the state signal is 0. However, the sigmoid function never reaches 0, confirming that the cooling can be fast transported to the RTD proximity. The bottom plot shows a considerable discrepancy between the hypothetical and local evaporator temperatures during the OFF and transition periods. The local evaporator temperature decays more slowly than the hypothetical one before the saturated period and becomes nearly identical when the sigmoid function reaches saturation. In addition, the hypothetical evaporator temperature peaks between consecutive ON periods.

The parameter C^e buffers this phenomenon such that the peaks of the local evaporator temperature are aligned to the compressor state shifts.



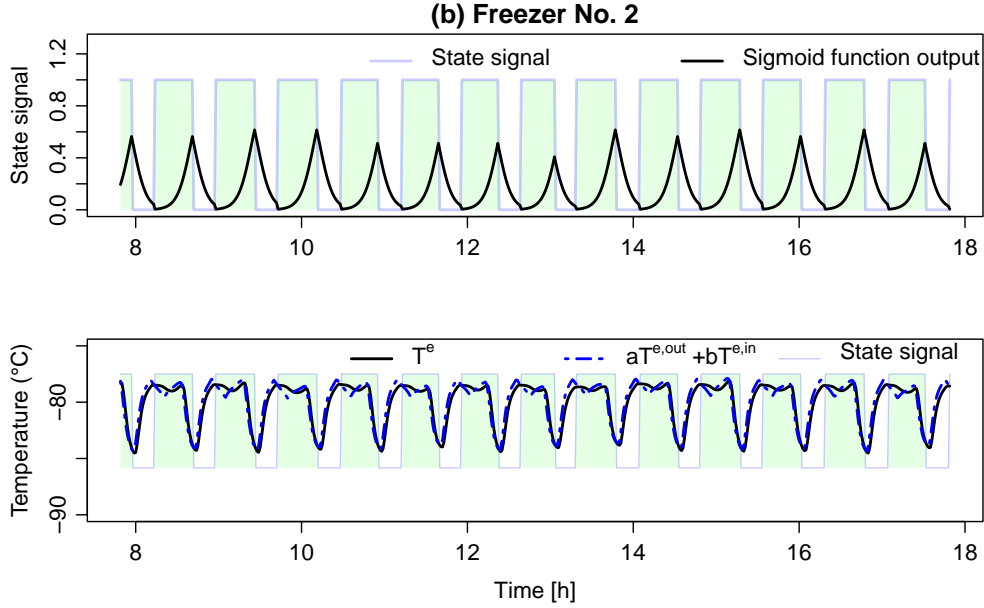


Fig. 7. Top: Correlation between the compressor state signal and output from the sigmoid function. Bottom: Comparison between the hypothetical evaporator temperature and estimated cold surface temperature. (a) for F#1 and (b) for F#2. The compressors are running during the square-shaded periods.

F#2 shows contrasting results compared F#1, as shown in Fig. 7 (b). The sigmoid function never reaches saturation, indicating that it always limits the changing of the local evaporator temperature towards the hypothetical evaporator temperature. This is confirmed in the bottom plot, in which the local evaporator temperature always slightly deviates from the hypothetical evaporator temperature. Although C^e is small for F#2, the lagging effect and their discrepancy are still noticeable, especially during the parts when the output of the sigmoid function is small. In both models, the hypothetical and the local evaporator temperature have a similar trend for both freezers, indicating that the linear assumption of the hypothetical evaporator temperature is reasonable. However, it is important to note that the comparison between the hypothetical and local evaporator temperatures is primarily intended to illustrate how the sigmoid function enables efficient prediction of time delays and reduced cooling capacity, while also providing insight into potential underlying phenomena that can be challenging to measure directly. It is not meant to imply that the modelled evaporator temperature represents the ground truth.

The effects of the sigmoid function are found to play a rather salient role in yielding good model predictions, particularly in the initial stage of the ON period. This confirms that modelling the cooling input as a smooth change is appropriate. This can be superficially explained by the fact that thermo-mechanical systems require a warming-up period to reach nominal conditions.

Whereas, such warming-up periods may not only depend upon the intrinsic properties of the systems but also be inevitably influenced by other factors such as loading and wear conditions. Therefore, the governing parameters (α and β) for the sigmoid function may vary for different freezers and even for the same freezers at different lifetimes. This reveals that any exact models for ULT freezers can risk limited applicability. In this light, the proposed grey-box modelling approach is scalable and more promising for practical applications.

4.5. Model identifiability

Fig. 8 displays the correlogram of the estimated parameters. The patterns of the correlation matrices for the two models are different, but fairly strong correlations ($|R| > 0.9$) can be found between some parameters. This is particularly clear for $M_{F\#2}$, in which strong correlations can be observed between thermal-related parameters C and R . It indicates that these parameters are not independent, and the model may not be practically identifiable.

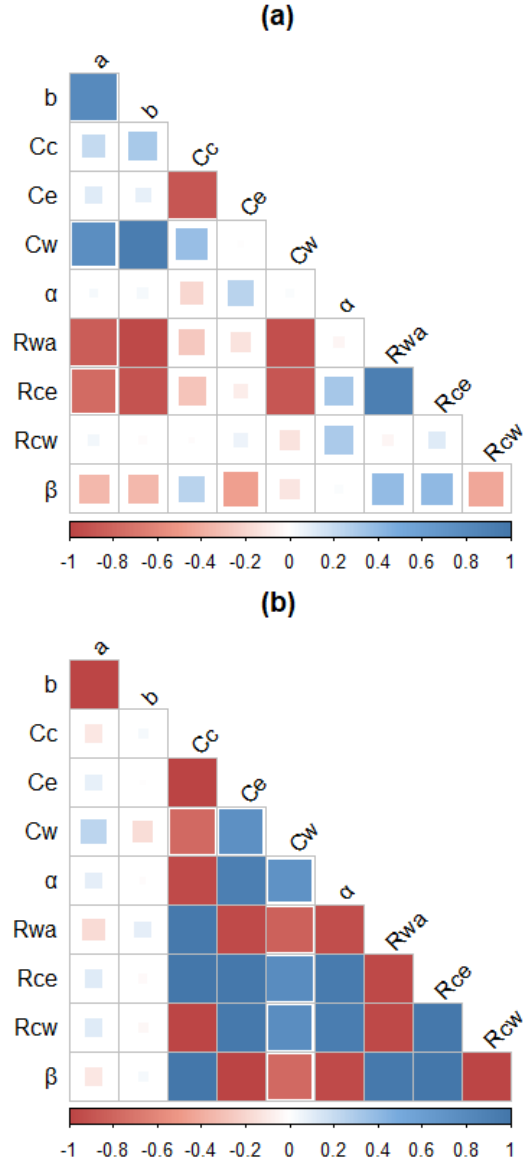


Fig. 8. Correlogram between estimated parameters. (a) F#1. (b) F#2.

We employ the profile likelihood to further evaluate the identifiability. Because of computationally burdensome, we only select C^c from $M_{F\#2}$ as the parameter of interest because it is highly correlated with other parameters. Fig. 9 shows the normalized profile log-likelihood for C^c in a solid line. The profile likelihood distribution is rather flat and always above the 95% confidence threshold, despite a reducing tendency at large C^c . This indicates that a similar level of maximum likelihood can be derived from a wide range of C^c . The dashed line in Fig. 9 plots the profile likelihood of C^c by keeping R^{ce} to be the estimated value $1.5e-2$. The profile likelihood distribution shows a well-defined confidence interval. This suggests that C^c and R^{ce} are dependent. This mutual dependency is confirmed by Fig. 9 (b), in which a clear relationship between the C^c and R^{ce} at the maximum log-likelihood is shown. The results suggest that the model is not practically identifiable

and imply that the classic quadratic assumption does not strictly hold for all parameters.

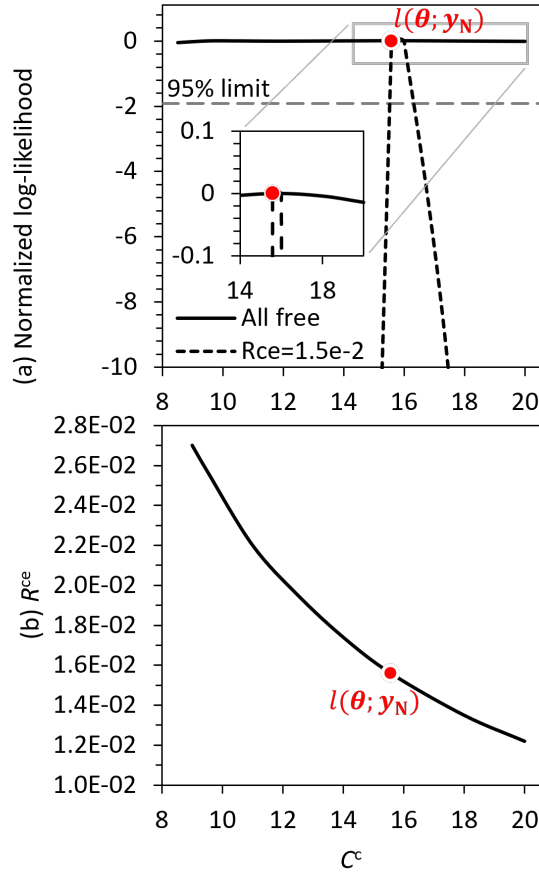


Fig. 9. (a) Profile likelihood estimated at different C^c with all other parameters remaining free and with $R^{ce} = 1.5e - 2$. (b) Correlation between C^c and R^{ce} derived at the maximum log-likelihood.

Identifiability is a crucial prerequisite to reliable parameter inference. The weak identifiability of the proposed models is mainly due to the absence of a dimension constraint in energy quantity. Additionally, the limited variability in the non-intrusive data used for identification can also contribute to weak identifiability, as shown in Fig. 2. The non-intrusive data may contain too little information on the system dynamics to achieve the unicity of each parameter estimation. Therefore, we should avoid interpreting them as the exact physical proprieties of the systems.

The results in Fig. 9 (b) point out a possible way to enhance the identifiability of the model, that is, to fix some of the parameters to be the true value to reduce the degree of the freedoms. This, however, requires domain knowledge and may entail demand for extra experiments. The less strong correlations between the parameters of $M_{F\#2}$ somewhat indicate more reliable parameter estimates, reflecting that specific dynamical patterns can also enhance the model identifiability. Another approach to improve the level of data information is through excitation of the system against a large spectrum

of frequencies using a periodic and deterministic pseudo-random binary sequence [24, 37, 42, 43]. However, this also requires controlled experiments and thus is not always accessible.

Although a fully interpretable model is desirable, it can be demanding to build and sustain in practical settings. Despite the lack of identifiability of the present model, it effectively captures the main heat dynamics of the system and can easily adapt to the system state changes through parameter re-estimation based on operational data. This feature strongly facilitates practical applications and maintenance of the model.

4.6. Long-term model performance

In practical operations, ULT freezers are subject to continuous external disturbances, which can lead to changes in chamber thermal properties and alter the dynamical behaviours. For instance, the heat capacity of the chamber can change due to loading activities. Frosting on the inner surface of the chamber can increase the thermal resistance. Consequently, a specific model will not maintain throughout the entire lifespan of an ULT freezer. It thus becomes necessary to update the model to capture the evolving heat dynamics of the freezing chamber when the previous dynamical equilibrium is disrupted.

Long-term unconditional predictions are conducted to elaborate on this issue. We selected a 4-month regular operational period of F#2, which included multiple door-opening events. Fig. 10 (a) shows the unconditional prediction residuals from the baseline model $M_{F\#2}$ over the 4 months. The residuals are centred along zero within a narrow span during the first 1.5 months when no external disturbance occurs. Afterwards, the residuals start to drift from zero, suggesting that the baseline model $M_{F\#2}$ underestimates the RTD temperature. Therefore, relevant parameters should be retuned to maintain the model performance.

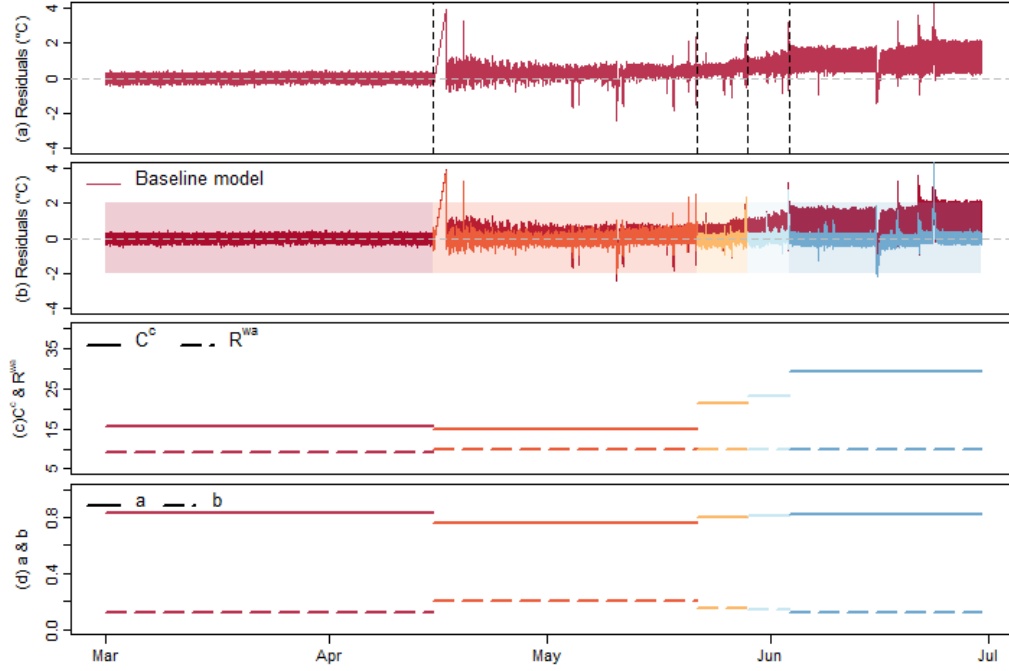


Fig. 10. (a) Temporal evolution of residuals from the baseline $M_{F\#2}$ from March to July. (b) Comparisons between the residuals from the baseline model and four retuned models. (c-d) retuned parameters for each model.

We then selected four events and divided the 4-month into five sub-periods, separated by the vertical dashed lines, see Fig. 10 (a). Apart from the first reboot event, all events were door-opening. We chose them because the residuals exhibit a clear tendency to drift from the previous level. There are also a few door-opening events within each sub-period reflected by the spikes in the residuals. However, they do not cause significant drift on the residuals and are thus not considered to demand parameter updates.

As discussed in Subsection 4.1, the C^w , C^e , R^{ce} , and R^{wa} values of $M_{F\#2}$ are more likely to be related to the intrinsic properties of the freezers, while C^c and R^{cw} are more easily affected by external disturbances. Thus, it is reasonable to retune only C^c and R^{cw} while fixing the remaining ones. a and b values also need to be retuned to adjust the contribution of the inlet and outlet temperatures to the local evaporator temperature. This partial retuning strategy can reduce computational time and improve the model identification stability.

Fig. 10 (b) presents the unconditional prediction residuals from the four updated models during each sub-period. The retuned models lead to a similar level of residuals as the baseline model. However, the residuals still spike at door-opening events. This is expected as the model does not account for infiltration and thus cannot effectively predict temperature evolution during door-opening events, which can heavily depend on random user behaviours [11]. Moreover, it may be less critical to reproduce the temperature profile during door-opening events, especially if these events are being logged.

Fig. 10 (c) shows the retuned C^c and R^{wa} values. C^c is relatively more sensitive to state changes. In contrast, the level of R^{cw} changes insignificantly. Fig. 10 (d) shows the retuned a and b values. The results suggest again that a and b are negatively correlated. The estimated a is smaller after the first event and gradually increases thereafter. Overall, the changes in a and b are small.

The results demonstrate that the freezers are subject to unpredictable changes in their dynamic behaviours over time. Therefore, updating the model is necessary to sustain its performance in the long run. This highlights the advantage of using a stochastic grey-box model, which allows the parameters to be easily tuned using measured time series data while considering stochasticity. Such flexibility greatly facilitates resilient online applications and decision-making under uncertainty.

Furthermore, the parameter retuning processes may provide an alternative approach to physical interpretation. The proposed model is built upon the heat transfer theory, ensuring the validity of the simulated heat transfer processes and the roles of the parameters within the model structure. Consequently, the parameters should function according to their definitions. Even though the absolute values of the parameters may lack meaning, their relative changes can potentially be interpreted based on their physical definitions. For instance, increasing levels of C^c in Fig. 10 (c) possibly indicate an increased mass of the contents in the chamber after each selected event. Changes in a and b can to an extent reflect the evaporation status in the evaporator. This relative parameter inference strategy can also offer valuable information on the operational status of ULT freezers and is promising to compensate for the low model identifiability. Unfortunately, the lack of detailed information about loading events hinders the validation of this strategy against the actual events. Experiments are necessary to confirm the effectiveness of this approach.

4.7. Potential applications and limitations

The developed modelling approach demonstrates strong prediction performance and transferability, serving several potential digital applications. One such application is continuous online surveillance, proven by model predictive performance and convenient parameter re-estimates. Consequently, the model can function as a residual generator through Kalman Filter for FDD purposes. Studies have reported that the innovation from the Kalman Filter can effectively detect subtle changes in the system states [44, 45, 46], which are challenging to identify through simple setpoint alarms alone. This capability contributes to early fault detection, leading to timely fault correction. Furthermore, good predictive performance and residual analysis evidence the potential for forecasting tasks. This ability makes the model qualified for MPC purposes, which is promising to reduce energy consumption from ULT freezers.

Several limitations of the present study must be made clear. First, the data used for the modelling processes comes from the ULT freezers with

2CRS. It is unclear whether the proposed modelling approach can be extrapolated to ULT freezers with other refrigeration systems, e.g. Auto-Cascading Refrigeration Systems [36]. Generalizing the results to other types of ULT and standard freezers would help to improve the understanding of their dynamic behaviour. Second, the availability of the evaporator inlet and outlet temperatures may vary among different brands of ULT freezers. However, it is increasingly common for multiple sensors to be installed in ULT freezers by several manufacturers. Also, measuring temperatures remain relatively easy and inexpensive that can be feasibly implemented in practice to facilitate the model applications. Thirdly, the relative parameter interpretation strategy suggested in Subsection 4.6 is not validated. A case study would be worthwhile to evaluate its effectiveness and practical applicability.

5. Conclusions

A reliable dynamic model is essential for intelligent surveillance and efficient energy management for ULT freezers. This study develops a novel approach to modelling the heat dynamics of the ULT freezing chamber based exclusively on costless data from the embedded sensors. The model consists of two fully linear states, RTD temperature and chamber wall temperature. In addition, a hidden state of the local evaporator temperature is formulated based on a sigmoid function and a modified compressor state signal, enabling for effective incorporation of time delays and reduced cooling capacity into the system. The established models are proven to accurately capture the dynamics of the RTD temperature in ULT freezers with different operational patterns. The unconditional predictions are in good agreement with the measurements, demonstrating its potential for continuous chamber temperature monitoring.

The proposed modelling approach significantly promotes the practical applicability and transferability of grey-box modelling of ULT freezing chambers, as no costly meters and intrusive experiments are required. More importantly, the ability to easily retune the parameters while considering uncertainties over time enables the model to maintain its reliable prediction performance throughout the entire lifespan of the ULT freezers. However, a major limitation is the low model identifiability, which hampers the direct association of model parameters with physical meaning. Addressing this issue by analyzing the relative changes observed during each model update holds promise and warrants further investigation. Future research will also focus on practical implementations of the model, such as FDD and MPC.

CRediT authorship contribution statement

Tao Huang: Conceptualization, Methodology, Software, Validation, Investigation, Visualization, Writing - Original Draft. **Peder Bacher:** Conceptualization, Supervision, Writing - review & editing, Funding acquisition, Project administration. **Jan Kloppenborg Møller:** Conceptualization, Supervision, Writing - review & editing. **Francesco D’Ettorre:** Resources,

Writing - review & editing. **Wiebke Brix Markussen:** Resources, Writing - review & editing, Project administration.

Declaration of Competing Interest

The authors declare that they have no known competing financial interests or personal relationships that could have appeared to influence the work reported in this paper.

Acknowledgment

This work was supported by the Danish Energy Technology Development and Demonstration Program (Grant No. 64021-1035). The authors appreciate Frederik Wulff Winthereik, and Jakob Thomsen from Danish Technological Institute for their support during the data collection.

Appendix A. Calculation of correlation matrix

Because the Maximum Likelihood estimator is an asymptotically Gaussian with mean $\boldsymbol{\theta}$ and covariance

$$\boldsymbol{\Sigma}_{\hat{\boldsymbol{\theta}}} = \mathbf{H}^{-1}, \quad (\text{A.1})$$

where, \mathbf{H} is the Hessian evaluated at the minimum of the objective function, i.e.

$$\{h_{ij}\} = -\left(\frac{\partial^2}{\partial\theta_i\partial\theta_j}l(\boldsymbol{\theta}; \mathbf{y}_N)\right)\Big|_{\boldsymbol{\theta}=\hat{\boldsymbol{\theta}}}, i, j = 1, \dots, p \quad (\text{A.2})$$

The correlation matrix \mathbf{R} can be obtained by decomposing the covariance matrix

$$\boldsymbol{\Sigma}_{\hat{\boldsymbol{\theta}}} = \boldsymbol{\sigma}_{\hat{\boldsymbol{\theta}}}\mathbf{R}\boldsymbol{\sigma}_{\hat{\boldsymbol{\theta}}}, \quad (\text{A.3})$$

where, $\boldsymbol{\sigma}_{\hat{\boldsymbol{\theta}}}$ is the diagonal matrix of the standard deviations of the estimated parameters.

References

- [1] Storage and Handling of Pfizer-BioNTech COVID-19 Vaccines, Technical Report, Center for Disease Control and Prevention (CDC), 2022. URL: <https://www.cdc.gov/vaccines/covid-19/info-by-product/pfizer/storage.html>.
- [2] M. Farley, B. McTeir, A. Arnott, A. Evans, Efficient ULT freezer storage, Technical Report, University of Edinburgh, 2015. URL: https://www.ed.ac.uk/files/atoms/files/efficient_ult_freezer_storage.pdf.

- [3] L. Kitzing, J. Katz, S. T. Schrönder, P. E. Morthorst, F. M. Andersen, The residential electricity sector in denmark: A description of current conditions, 2016. URL: https://orbit.dtu.dk/files/121099206/The_residential_electricity_sector_in_Denmark.pdf.
- [4] L. A. M. Gumapas, G. Simons, Factors affecting the performance, energy consumption, and carbon footprint for ultra low temperature freezers: case study at the national institutes of health, *World Review of Science, Technology and Sustainable Development* 10 (2013) 129–141. doi:<https://doi.org/10.1504/WRSTSD.2013.050786>.
- [5] Plug load test for ULT Freezers : 20-22% lower energy consumption at -70 °C compared to -80 °C, Technical Report, Copenhagen University, 2017. URL: <https://baeredygtighed2030.ku.dk/pdf/frysertest.pdf>.
- [6] N. O’Connell, P. Pinson, H. Madsen, M. O’Malley, Benefits and challenges of electrical demand response: A critical review, *Renewable and Sustainable Energy Reviews* 39 (2014) 686–699. doi:<https://doi.org/10.1016/j.rser.2014.07.098>.
- [7] F. D’Ettorre, M. Banaei, R. Ebrahimi, S. A. Pourmousavi, E. Blomgren, J. Kowalski, Z. Bohdanowicz, B. Lopaciuk Gonczaryk, C. Biele, H. Madsen, Exploiting demand-side flexibility: State-of-the-art, open issues and social perspective, *Renewable and Sustainable Energy Reviews* 165 (2022) 112605. doi:<https://doi.org/10.1016/j.rser.2022.112605>.
- [8] R. Legett, Field Demonstration of High-Efficiency Ultra-Low-Temperature Laboratory Freezers, Technical Report, U.S. Department of Energy, 2014. URL: <https://www.energy.gov/eere/buildings/articles/field-demonstration-high-efficiency-ultra-low-temperature-laboratory>.
- [9] M. Schwenzer, M. Ay, T. Bergs, D. Abel, Review on model predictive control: an engineering perspective, *The International Journal of Advanced Manufacturing Technology* 117 (2021) 1327–1349. doi:<https://doi.org/10.1007/s00170-021-07682-3>.
- [10] S. Yang, M. P. Wan, B. F. Ng, S. Dubey, G. P. Henze, W. Chen, K. Baskaran, Model predictive control for integrated control of air-conditioning and mechanical ventilation, lighting and shading systems, *Applied Energy* 297 (2021) 117112. doi:<https://doi.org/10.1016/j.apenergy.2021.117112>.
- [11] R. Mastrullo, A. Mauro, L. Menna, A. Palma, G. Vanoli, Transient model of a vertical freezer with door openings and defrost effects, *Applied Energy* 121 (2014) 38–50. doi:<https://doi.org/10.1016/j.apenergy.2014.01.069>.

- [12] G. Zsembinszki, A. de Gracia, P. Moreno, R. Rovira, M. Ángel González, L. F. Cabeza, A novel numerical methodology for modelling simple vapour compression refrigeration system, *Applied Thermal Engineering* 115 (2017) 188–200. doi:<https://doi.org/10.1016/j.applthermaleng.2016.12.059>.
- [13] Y. Li, X. Pan, X. Liao, Z. Xing, A data-driven energy management strategy based on performance prediction for cascade refrigeration systems, *International Journal of Refrigeration* 136 (2022) 114–123. doi:<https://doi.org/10.1016/j.ijrefrig.2022.01.012>.
- [14] S. Srinivasan, A. Vasan, V. Sarangan, A. Sivasubramaniam, Bugs in the freezer: Detecting faults in supermarket refrigeration systems using energy signals, in: *Proceedings of the 2015 ACM Sixth International Conference on Future Energy Systems, e-Energy '15*, Association for Computing Machinery, New York, NY, USA, 2015, p. 101–110. URL: <https://doi.org/10.1145/2768510.2768536>. doi:<https://doi.org/10.1145/2768510.2768536>.
- [15] M. Hosoz, H. M. Ertunc, Modelling of a cascade refrigeration system using artificial neural network, *International Journal of Energy Research* 30 (2006) 1200–1215. doi:<https://doi.org/10.1002/er.1218>.
- [16] A. Afram, F. Janabi-Sharifi, Review of modeling methods for hvac systems, *Applied Thermal Engineering* 67 (2014) 507–519. doi:<https://doi.org/10.1016/j.applthermaleng.2014.03.055>.
- [17] Y. Zong, G. M. Böning, R. M. Santos, S. You, J. Hu, X. Han, Challenges of implementing economic model predictive control strategy for buildings interacting with smart energy systems, *Applied Thermal Engineering* 114 (2017) 1476–1486. doi:<https://doi.org/10.1016/j.applthermaleng.2016.11.141>.
- [18] R. De Coninck, L. Helsen, Practical implementation and evaluation of model predictive control for an office building in brussels, *Energy and Buildings* 111 (2016) 290–298. doi:<https://doi.org/10.1016/j.enbuild.2015.11.014>.
- [19] C. A. Thilker, R. G. Junker, P. Bacher, J. B. Jørgensen, H. Madsen, *Model Predictive Control Based on Stochastic Grey-Box Models*, Springer International Publishing, 2021, pp. 329–380. doi:https://doi.org/10.1007/978-3-030-76477-7_11.
- [20] S. Rouchier, M. Rabouille, P. Oberlé, Calibration of simplified building energy models for parameter estimation and forecasting: Stochastic versus deterministic modelling, *Building and Environment* 134 (2018) 181–190. doi:<https://doi.org/10.1016/j.buildenv.2018.02.043>.

- [21] Z. O'Neill, S. Narayanan, Model-based estimation of cold room temperatures in a supermarket refrigeration system, *Applied Thermal Engineering* 73 (2014) 819–830. doi:<https://doi.org/10.1016/j.applthermaleng.2014.08.038>.
- [22] K. Leerbeck, P. Bacher, C. Heerup, Grey box modelling of supermarket refrigeration room, in: 2021 International Conference on Electrical, Computer and Energy Technologies (ICECET), 2021, pp. 1–6. doi:10.1109/ICECET52533.2021.9698514.
- [23] K. Leerbeck, P. Bacher, C. Heerup, H. Madsen, Grey box modeling of supermarket refrigeration cabinets, *Energy and AI* 11 (2023) 100211. doi:<https://doi.org/10.1016/j.egyai.2022.100211>.
- [24] F. Sossan, V. Lakshmanan, G. T. Costanzo, M. Marinelli, P. J. Douglass, H. Bindner, Grey-box modelling of a household refrigeration unit using time series data in application to demand side management, *Sustainable Energy, Grids and Networks* 5 (2016) 1–12. doi:<https://doi.org/10.1016/j.segan.2015.10.003>.
- [25] G. T. Costanzo, F. Sossan, M. Marinelli, P. Bacher, H. Madsen, Grey-box modeling for system identification of household refrigerators: A step toward smart appliances, in: 2013 4th International Youth Conference on Energy (IYCE), 2013, pp. 1–5. doi:<https://doi.org/10.1109/IYCE.2013.6604197>.
- [26] Z. Liu, M. Bai, H. Tan, Y. Ling, Z. Cao, Experimental test on the performance of a -80 °c cascade refrigeration unit using refrigerants r290-r170 for covid-19 vaccines storage, *Journal of Building Engineering* 63 (2023) 105537. doi:<https://doi.org/10.1016/j.jobbe.2022.105537>.
- [27] H. Tan, L. Xu, L. Yang, M. Bai, Z. Liu, Operation performance of an ultralow-temperature cascade refrigeration freezer with environmentally friendly refrigerants r290-r170, *Environmental Science and Pollution Research* (2022). doi:<https://doi.org/10.1007/s11356-022-24310-z>.
- [28] S. Bhattacharyya, A. Garai, J. Sarkar, Thermodynamic analysis and optimization of a novel n2o-co2 cascade system for refrigeration and heating, *International Journal of Refrigeration* 32 (2009) 1077–1084. doi:<https://doi.org/10.1016/j.ijrefrig.2008.09.008>.
- [29] A. Kilicarslan, M. Hosoz, Energy and irreversibility analysis of a cascade refrigeration system for various refrigerant couples, *Energy Conversion and Management* 51 (2010) 2947–2954. doi:<https://doi.org/10.1016/j.enconman.2010.06.037>.
- [30] Z. Sun, Y. Liang, S. Liu, W. Ji, R. Zang, R. Liang, Z. Guo, Comparative analysis of thermodynamic performance of a cascade refrigeration system for refrigerant couples r41/r404a and r23/r404a, *Applied*

- Energy 184 (2016) 19–25. doi:<https://doi.org/10.1016/j.apenergy.2016.10.014>.
- [31] Z. Sun, Q. Wang, Z. Xie, S. Liu, D. Su, Q. Cui, Energy and exergy analysis of low gwp refrigerants in cascade refrigeration system, Energy 170 (2019) 1170–1180. doi:<https://doi.org/10.1016/j.energy.2018.12.055>.
- [32] J. A. Dopazo, J. Fernández-Seara, Experimental evaluation of a cascade refrigeration system prototype with co2 and nh3 for freezing process applications, International Journal of Refrigeration 34 (2011) 257–267. doi:<https://doi.org/10.1016/j.ijrefrig.2010.07.010>.
- [33] C. Sanz-Kock, R. Llopis, D. Sánchez, R. Cabello, E. Torrella, Experimental evaluation of a r134a/co2 cascade refrigeration plant, Applied Thermal Engineering 73 (2014) 41–50. doi:<https://doi.org/10.1016/j.applthermaleng.2014.07.041>.
- [34] R. Llopis, D. Sánchez, C. Sanz-Kock, R. Cabello, E. Torrella, Energy and environmental comparison of two-stage solutions for commercial refrigeration at low temperature: Fluids and systems, Applied Energy 138 (2015) 133–142. doi:<https://doi.org/10.1016/j.apenergy.2014.10.069>.
- [35] Y.-D. Zhu, Z.-R. Peng, G.-B. Wang, X.-R. Zhang, Thermodynamic analysis of a novel multi-target-temperature cascade cycle for refrigeration, Energy Conversion and Management 243 (2021) 114380. doi:<https://doi.org/10.1016/j.enconman.2021.114380>.
- [36] M. Pan, H. Zhao, D. Liang, Y. Zhu, Y. Liang, G. Bao, A review of the cascade refrigeration system, Energies 13 (2020) 2254. doi:<https://doi.org/10.3390/en13092254>.
- [37] H. Madsen, J. Holst, Estimation of continuous-time models for the heat dynamics of a building, Energy and Buildings 22 (1995) 67–79. doi:[https://doi.org/10.1016/0378-7788\(94\)00904-X](https://doi.org/10.1016/0378-7788(94)00904-X).
- [38] P. Frogerais, J.-J. Bellanger, L. Senhadji, Various ways to compute the continuous-discrete extended kalman filter, IEEE Transactions on Automatic Control 57 (2012) 1000–1004. doi:<https://doi.org/10.1109/TAC.2011.2168129>.
- [39] B. Øksendal, Stochastic Differential Equations - An Introduction with Applications, Universitext, Springer Berlin, Heidelberg, 1985.
- [40] N. R. Kristensen, H. Madsen, S. B. Jørgensen, Parameter estimation in stochastic grey-box models, Automatica 40 (2004) 225–237. doi:<https://doi.org/10.1016/j.automatica.2003.10.001>.

- [41] H. Madsen, P. Thyregod, *Introduction to General and Generalized Linear Models* (1st ed.), CRC Press, 2010. doi:<https://doi.org/10.1201/9781439891148>.
- [42] P. Bacher, H. Madsen, Identifying suitable models for the heat dynamics of buildings, *Energy and Buildings* 43 (2011) 1511–1522. doi:<https://doi.org/10.1016/j.enbuild.2011.02.005>.
- [43] X. Yu, L. Georges, L. Imsland, Data pre-processing and optimization techniques for stochastic and deterministic low-order grey-box models of residential buildings, *Energy and Buildings* 236 (2021) 110775. doi:<https://doi.org/10.1016/j.enbuild.2021.110775>.
- [44] Z. Yang, K. B. Rasmussen, A. T. Kieu, R. Izadi-Zamanabadi, Fault detection and isolation for a supermarket refrigeration system – part one: Kalman-filter-based methods, *IFAC Proceedings Volumes* 44 (2011) 13233–13238. doi:<https://doi.org/10.3182/20110828-6-IT-1002.03115>, 18th IFAC World Congress.
- [45] A. Okatan, C. Hajiyev, U. Hajiyeva, Fault detection in sensor information fusion kalman filter, *AEU - International Journal of Electronics and Communications* 63 (2009) 762–768. doi:<https://doi.org/10.1016/j.aeue.2008.06.003>.
- [46] P. Jieyang, A. Kimmig, W. Dongkun, Z. Niu, F. Zhi, W. Jiahai, X. Liu, J. Ovtcharova, A systematic review of data-driven approaches to fault diagnosis and early warning, *Journal of Intelligent Manufacturing* (2022). doi:<https://doi.org/10.1007/s10845-022-02020-0>.